RSC Advances

ROYAL SOCIETY OF CHEMISTRY

www.rsc.org/advances

Modification of alkaline-earth oxides (MgO, CaO, SrO and BaO) to Ni/SiO_2 catalyst could affect significantly the reducibility of the Ni species under given reaction conditions (450 °C, H_2/Ar molar ratio = 1/19, Flow rate = 40 ml min^{-1}, and P = 1 atm).

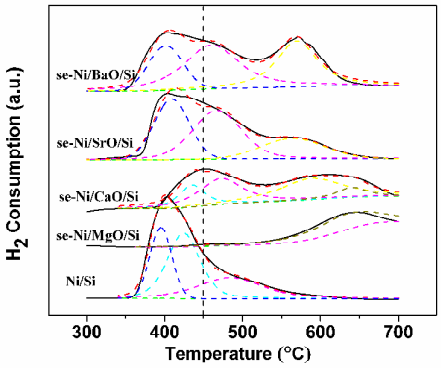

The difference of roles of alkaline-earth metal oxides on silica-supported nickel catalysts for CO_2 methanation

Meng Guo [a,b], Gongxuan Lu [a,*]

[a] State Key Laboratory for Oxo Synthesis and Selective Oxidation, Lanzhou Institute of Chemical Physics, Chinese Academy of Sciences, Lanzhou 730000, P.R. China

[b] University of Chinese Academy of Sciences, Beijing 100049, P.R. China

* Corresponding author. Tel.: +86 931 4968178

E-mail address: gxlu@lzb.ac.cn (G. Lu)

Abstract

The roles of alkaline-earth metal oxides on CO_2 methanation over modified Ni/SiO_2 catalysts were investigated. $Ni/MO/SiO_2$ catalysts with variable elements (M = Mg, Ca, Sr and Ba) were prepared by the sequential impregnation method. The results indicated that the presence of SrO promoted the catalytic activity and enhanced the catalyst stability. In addition, BaO addition enhanced the reaction activity, but $Ni/BaO/SiO_2$ catalyst deactivated significantly after 50 h of time-on-stream due to the sintering of metallic Ni. Besides, CaO addition affected negligibly the performance of $Ni/CaO/SiO_2$ catalyst, and MgO addition inhibited significantly the methanation performance because of the low reducibility of Ni species.

Keywords Methanation · Supported nickel · Alkaline-earth metal oxide · CO_2 · Stability

1 Introduction

Nowadays, the ~395 ppm level of CO_2 in the atmosphere has caused a lot of severe environmental problems. To mitigate them, capture and conversion of CO_2 have been investigated extensively. The process related with CO_2 chemical utilization such as providing various commodity chemicals and renewable fuels has been proposed [1-9]. It is well known that methane as a renewable fuel can be produced from the Sabatier reaction, i.e., hydrogenation of CO_2 to methane. If hydrogen in this reaction is provided by solar energy, for example, *via* water photolysis, the sustainable cycle can be achieved.

The Ru, Rh and Pd catalysts supported on Al_2O_3, TiO_2 and MgO etc., have exhibited excellent catalytic properties in CO_2 methanation [5,10-12], among which Ru is the best active component at low temperature [13]. Some supported or non-supported transition metal catalysts have acceptable performances, such as Ni [8,9,14-19], Co [20-23] and Fe [20,24]. Moreover, the promotion effect of second transition metal addition to the Ni-based catalysts have also been reported [25,26]. If a proper amount of Mo is added to the Ni-based catalysts, both the catalytic activity and selectivity of CH_4 can be enhanced. It can be attributed to the formation of MoOx species, which not only promotes Ni metal particle dispersion, but also helps the partial electron transfer to Ni sites [25].

Depending on the catalytic system considered, alkaline-earth metal oxides act as structural promoters by increasing the dispersion of the active phase and stabilizing the dispersed metallic phase against sintering [19,27-29]. In addition, these additives also act as chemical promoters by influencing the acid–base properties of support [30-32] or the electron density of dispersed metal crystallites [33,34]. Park et al. have revealed that MgO can initiate the reaction by binding CO_2 molecules *via* forming

magnesium carbonate species on the catalyst surface. The supply of hydrogen atoms is essential for hydrogenation of magnesium carbonate to CH_4 [30,31].

In this paper, the effect of alkaline-earth metal oxides (MgO, CaO, SrO and BaO) with the same controlled contents of Ni/SiO_2 catalyst for CO_2 methanation. The results indicated that the effect of alkaline-earth metal oxides was quite different. Therefore, the results were discussed by considering the roles of alkaline-earth metal-induced alterations of Ni/SiO_2 catalyst on the physicochemical characteristics. Moreover, the catalytic activity and catalyst stability were also discussed to develop the catalysts with enhanced activity and stability.

2 Experimental

2.1 Catalyst Preparation

Using $Ni(NO_3)_2 \cdot 6\ H_2O$ as a metal precursor, 10 wt.% Ni/SiO_2 (denoted as Ni/Si) catalyst was prepared by the wet impregnation followed by spontaneous dispersion upon calcination. Prior to impregnation, the support SiO_2 (20–45 mesh) was calcined 500 °C for 6 h. After calcination, its specific area was 438 m^2/g. The aqueous solution containing appropriate amount of $Ni(NO_3)_2$ was mixed with the calculated amount of support. After the impregnation for 24 h, the precursor mixture was dried further at 110 °C for another 24 h, and then calcined at 500 °C for 6 h in an oven.

10 wt.% Ni/4 wt.% MO/SiO_2 (M = Mg, Ca, Sr and Ba) catalysts were denoted as se-Ni/M/Si catalysts and prepared by the sequential impregnation method, in which impregnation of aqueous solution containing appropriate amount of $Mg(NO_3)_2$, $Ca(NO_3)_2$, $Sr(NO_3)_2$, or $Ba(NO_3)_2$ was followed by heat treatment and then by impregnation of nickel nitrate aqueous solution [35]. The two drying and calcination procedures were the same as for Ni/Si catalyst.

2.2 Catalytic Activity Measurements

The catalytic performance was carried out in a fixed bed continuous flow quartz reactor (i.d. 8 mm) using a mixture of H_2 and CO_2 at molar ratio of 4 balanced with N_2 (30 ml min^{-1}), which was depicted in Fig. 1. Typically, 0.2 g of catalyst was used in each turn at GHSV of 15000 ml h^{-1} g^{-1}. Previous to test, the fresh catalyst was reduced *in situ* for 3 h under a 50 vol.% H_2/N_2 mixture (60 ml min^{-1}) and then cooled down to room temperature under the same conditions. The effluent mixed gases were cooled in an ice-water trap to remove the gaseous water generated. The effluent gases were collected after half an hour of steady-state operation, and the separation and quantification of them were attained on two on-line chromatographs equipped with thermal-conductivity detectors (TCD). Nitrogen was used as a carrier gas and internal standard for gas analysis. Experimental error was typically within ±4%. The conversion of CO_2 and the selectivity to the products were calculated based on the balance of carbon, which was estimated within 100±1%. CO_2 conversion (X_{CO_2}), CH_4 selectivity (S_{CH_4}) and CO selectivity (S_{CO}) were described as follows:

$$X_{CO_2} = (F_{CO_2in} - F_{CO_2out})/F_{CO_2in} \quad (1)$$

$$S_{CH_4} = F_{CH_4out}/(F_{CH_4out} + F_{COout}) \quad (2)$$

$$S_{CO} = F_{COout}/(F_{CH_4out} + F_{COout}) \quad (3)$$

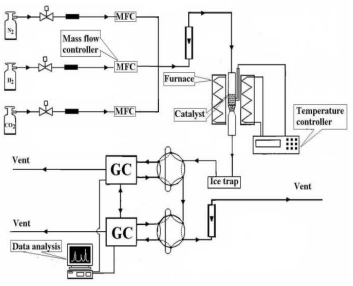

Fig. 1 Schematic diagram of the experimental system.

2.3 Catalyst Characterization

Hydrogen-temperature programmed reduction (H_2-TPR) measurements were carried out by heating a sample (50 mg) at 10 °C min^{-1} in a flow 5 vol.% H_2/Ar gas mixture (40 ml min^{-1}). The amount of consumed hydrogen was measured by a TCD.

X-ray diffraction (XRD) was performed on the selected samples using Cu Kα radiation (Philips X'pert MPD instrument) at a scattering rate of 4 °/min at 40 mA and 50kV.

Chemical states of the atoms on the catalyst surface were investigated by X-ray photoelectron spectroscopy (XPS) on a VG ESCALAB 210 Electron Spectrometer (Mg Kα radiation; hν = 1253.6 ev). XPS data were calibrated using the binding energy of the Si 2p (103.4 eV) as the standard.

Transmission electron microscopy (TEM) images were performed on the FEI F20 (Netherlands) high-resolution transmission electron microscopy operating at accelerating voltage of 200 kV. The sample for TEM analyses was sonicated in ethanol and then transferred as a suspension to carbon-coated copper grid.

3 Results and Discussion

3.1 H_2-TPR Analysis

H_2-TPR measurements were conducted to understand the reduction behavior of metal oxide-based supported catalysts, which could further provide information about the interactions between metal oxides and their supports. Profiles of H_2-TPR for the as-synthesized bare and modified Ni/SiO_2 materials were presented in Fig. 2 and the quantitative data of Ni species were given in Table 1, where significant effects of alkaline-earth metal oxides on the reduction behavior of the Ni species were observed.

TPR profile of Ni/Si catalyst was composed of a sharp peak and a shoulder peak. This sharp peak consisted of two maxima at 395 (α peak, 27%) and 424 °C (β peak, 43%), respectively. The two peaks were attributed to the reduction of some inhomogeneous NiO phases that interacted weakly with the silica [26,37]. The shoulder peak at 484 °C (γ peak, 30%) could be attributed to the stronger interactions between the bulk NiO phase and the support [38,39]. The initial reduction temperature was increased from 350 °C of Ni/Si catalyst to 440 °C of se-Ni/Mg/Si catalyst, 385°C of se-Ni/Ca/Si catalyst, and 365°C of se-Ni/Sr/Si catalyst. In addition, for all the modified Ni/SiO_2 catalysts, the reduction peaks of alkaline-earth metal-modified Ni/SiO_2 materials migrated gradually toward higher temperatures. For se-Ni/Mg/Si sample, the peaks were constituted by two maxima at 456 (γ peak, 1%) and 634 °C (ε peak, 99%), respectively. And then, for se-Ni/Ca/Si material, two broad reduction peaks was observed, which consisted of different peaks at 435 (β peak, 17%), 472 (γ peak, 34%), 588 (δ peak, 31%) and 640 °C (ε peak, 9%). In addition, the H_2-uptake ratios of Ni/Si, se-Ni/Mg/Si and se-Ni/Ca/Si catalysts were 1:0.3:0.8. For se-Ni/Sr/Si and se-Ni/Ba/Si catalysts, H_2-TPR profiles were similar and the area of the high temperature peaks increased obviously, which indicated that the amount of more stable Ni species increased. In addition, the H_2-uptake ratios of Ni/Si, se-Ni/Sr/Si and se-Ni/Ba/Si catalysts were 1:1.1:1.3.

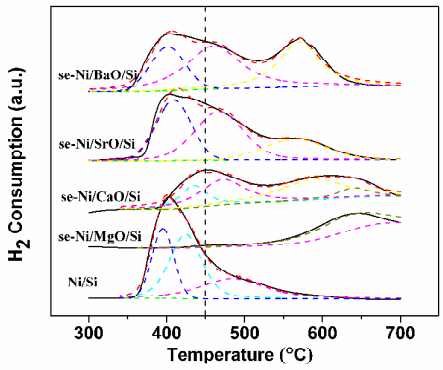

Fig. 2 H_2-TPR profiles of fresh catalysts.

Table 1 H_2-TPR quantitative data of fresh catalysts.

Samples	T_m (°C)					Fraction of total area (%)				
	α	β	γ	δ	ε	α	β	γ	δ	ε
Ni/Si	395	424	484	–	–	27	43	30	–	–
se-Ni/Mg/Si	–	–	456	–	634	–	–	1	–	99
se-Ni/Ca/Si	–	435	472	588	640	–	17	34	31	9
se-Ni/Sr/Si	409	–	467	564	–	35	–	44	24	–
se-Ni/Ba/Si	401	–	460	569	–	21	–	45	30	–

3.2 XRD Analysis

XRD patterns of bare and modified Ni/SiO_2 catalysts pretreated in a 50 vol.% H_2/N_2 mixture (60 ml min^{-1}) at 450 °C for 3 h were presented in Fig. 3. The typical broad diffraction peaks of SiO_2 support could be observed. For Ni/Si catalyst, the diffraction peaks located at 2θ = 44.5, 51.8 and 76.4° (JCPDC Card No. 87-0712), indicated the existence of the characteristics of Ni metal phase [17,40]. The NiO peaks were located at 2θ = 37.2, 43.3 and 62.8° (JCPDC Card No. 89-5881), which suggested that some NiO species existed in the bulk phase of catalysts [19,41]. In addition, the relative intensity of diffraction peaks of metallic Ni and NiO phases was 5.76. The diffraction peaks of Ni metal were very sharp, which indicated that Ni crystal phases were comparatively well crystallized. By comparison of Mg-modified Ni/SiO_2 catalyst, it was found that the XRD peaks could be attributed to NiO and MgO mixed phases (near 37.2, 43.3 and 62.8°, JCPDC Card No. 03-0988) and small amounts of Ni phase (near 44.5, 51.8 and 76.4°). For the se-Ni/Ca/Si, se-Ni/Sr/Si and se-Ni/Ba/Si catalysts, the relative intensities of diffraction peaks of metallic Ni and NiO phases were 0.97, 3.42 and 4.19, respectively, which suggested that Ni species over alkaline-earth metal-modified Ni/SiO_2 catalysts were more difficult to be

reduced than those over Ni/Si catalyst under some given conditions. Besides, there were $Ba_4Si_6O_{16}$ diffraction peak on the se-Ni/Ba/Si catalyst. In addition, the metallic Ni particle sizes on the Ni/Si, se-Ni/Mg/Si se-Ni/Ca/Si, se-Ni/Sr/Si and se-Ni/Ba/Si catalysts estimated from XRD of the peaks at $2\theta = 44.5^{\circ}$ calculated by the Scherrer formula were 50.9, 19.6, 35.8, 36.9 and 45.2 nm, respectively. It demonstrated that alkaline-earth metal oxides enhanced the dispersion of nickel species.

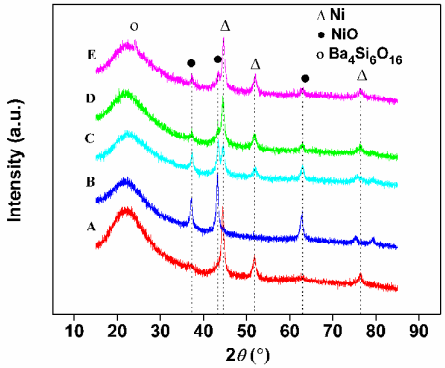

Fig. 3 XRD results of catalysts reduced at 450 °C: A, Ni/Si; B, se-Ni/Mg/Si; C, se-Ni/Ca/Si; D, se-Ni/Sr/Si; E, se-Ni/Ba/Si.

3.3 XPS Analysis

The chemical element states of surface species on the materials could be investigated commonly by XPS experiment. Therefore, XPS measurement was performed. The results related with binding energies of Ni $2p_{3/2}$ and the derived atomic composition in the different samples were analyzed and summarized in Fig. 4 and Table 2, respectively. It could be found that the binding energies of the surface Ni $2p_{3/2}$ species were affected significantly by modified alkaline-earth metal oxides. Moreover, the relative contents of nickel species changed significantly, as shown in Table 2. For the modified catalysts, the peaks of binding energies of Ni $2p_{3/2}$ were

mainly distributed around 853.8, 854.8 and 856.1 eV, which could be assigned to different types of NiO species [42]. The two higher binding energies of Ni $2p_{3/2}$ (around 858 and 863 eV) could be assigned to the shake-up satellite peaks of NiO species. Over Ni/Si catalyst surface, 49.3% NiO(γ) species was dominant. For se-Ni/Mg/Si and se-Ni/Ca/Si catalysts, the NiO(γ) species contents could increase to 49.6 and 62.5%, respectively. However, for se-Ni/Sr/Si and se-Ni/Ba/Si catalysts, the NiO(γ) species contents could decrease to 34.0 and 29.9%, respectively. The XPS results of samples in Table 2 demonstrated that Ni species increased on the modified catalyst surface with the modification of alkaline-earth metal oxides, as observed by the higher surface Ni/Si. Furthermore, the change of surface Ni/M (M = Mg, Ca, Sr or Ba) also indicated that the modified alkaline-earth metal oxides could be dispersed effectively on the SiO_2 support.

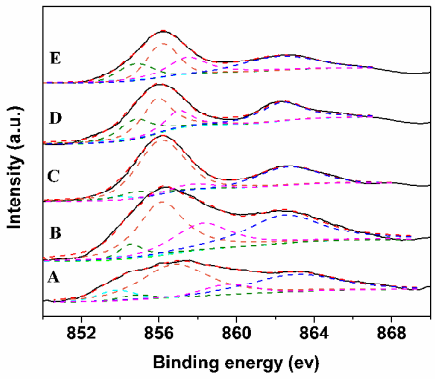

Fig. 4 XPS spectra of Ni $2p_{3/2}$ over fresh catalysts: A, Ni/Si; B, se-Ni/Mg/Si; C, se-Ni/Ca/Si; D, se-Ni/Sr/Si; E, se-Ni/Ba/Si.

Table 2 XPS results of fresh catalysts.

Samples	B.E. (Ni $2p_{3/2}$) (eV)					Fraction of total area (%)					Ni/Si[a]	M/Si[a]
	α	β	γ	δ	ε	α	β	γ	δ	ε		
Ni/Si	853.8	854.8	856.8	859.5	863.0	7.1	2.8	49.3	9.4	31.3	0.015	0

se-Ni/Mg/Si	853.8	854.8	856.1	859.6	862.8	6.7	2.9	49.6	8.2	30.5	0.034	0.120
se-Ni/Ca/Si	853.8	854.8	856.1	857.7	862.7	1.7	7.1	62.5	4.9	23.7	0.044	0.144
se-Ni/Sr/Si	853.8	854.8	855.9	857.0	862.4	2.9	20.7	34.0	15.0	27.4	0.056	0.088
se-Ni/Ba/Si	853.8	854.8	856.2	857.5	862.3	1.6	15.9	29.9	24.7	27.9	0.047	0.071

[a] Calculated by Ni (or M = Mg, Ca, Sr or Ba) atom% / Si atom% from XPS spectra.

3.4 Study of GHSV over Ni/Si Catalyst

Prior to all the catalytic experiments, a blank test was carried out firstly and did not show any catalytic activity, even at temperatures as high as 500 °C. Then, in order to optimize the catalyst amount loaded into the reactor, GHSV was ranged from 7500 to 60000 ml h^{-1} g^{-1}. The catalytic performances of Ni/Si catalyst under typical reaction conditions (H_2/CO_2 molar ratio = 4; P = 1 atm) were tested at these GHSV and temperatures ranging from 200 to 500 ^oC. The results of CO_2 conversions and product distributions were present in Fig. 5. As shown in Fig. 5a, when the reaction temperature was below 300 ^oC, the conversions were less than 50.6%. With the reaction temperature increased to 400 ^oC, CO_2 conversions ended up at 49.1, 61.3, 70.9, 73.2, 77.4 and 81.3% over CHSV of 60000, 30000, 20000, 15000, 10000 and 7500 ml h^{-1} g^{-1}, respectively. Moreover, at 350 and 400 ^oC and GHSV of 10000 ml h^{-1} g^{-1}, the similar CO_2 conversions were 74.9 and 77.4%, respectively, which indicated that working at 350 ^oC was optimal considering CH_4 selectivities and the high temperature sintering of the metallic Ni [43].

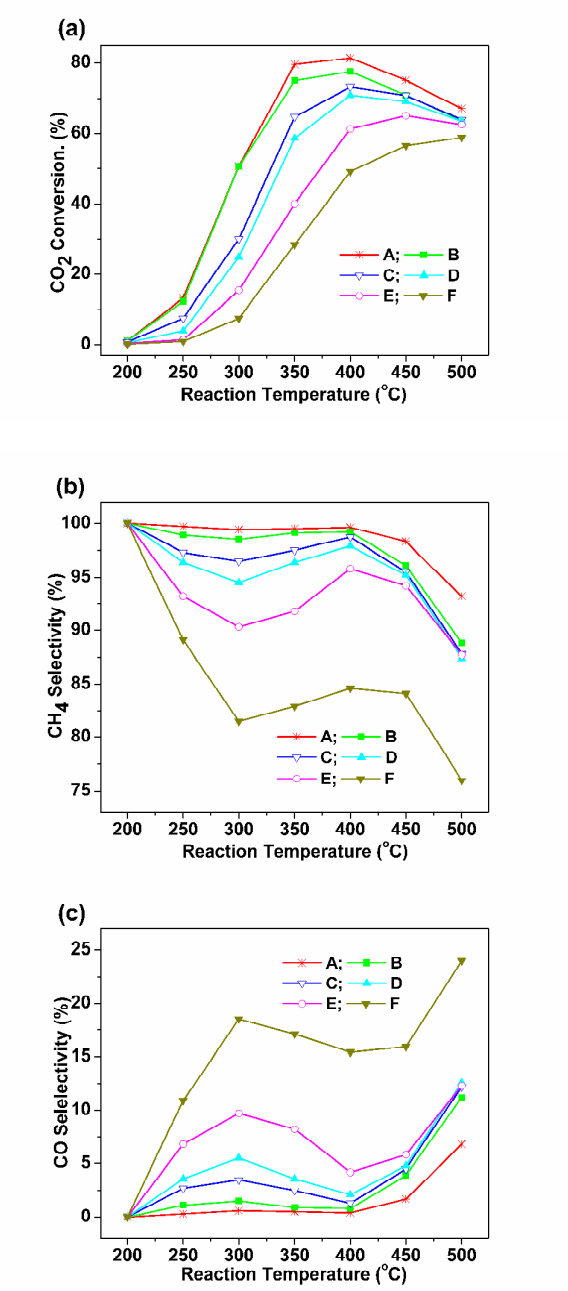

Fig. 5 Catalytic performance of Ni/Si catalyst at various temperatures and different GHSV: A, 7500; B, 10000; C, 15000; D, 20000; E, 30000; F, 60000 ml h^{-1} g^{-1}. Reaction conditions: H_2/CO_2 molar ratio = 4; P = 1 atm.

3.5 Catalytic performances over alkaline-earth metal-modified Ni/SiO_2 catalysts

The catalytic performances of the bare and modified Ni/SiO_2 catalysts were

investigated at temperatures ranging from 300 to 450 °C under the given reaction conditions (GHSV = 15000 ml h^{-1} g^{-1}, H_2/CO_2 molar ratio = 4 and P = 1 atm). Reaction temperature influenced significantly the catalytic behaviors [15-24]. As shown in Table 3, CO_2 conversions depended largely on the reaction temperatures. At 350 °C, carbon dioxide conversions were low and the reaction produced mostly CH_4 with small amounts of by-product CO [43,44]. With temperature increased to 450 °C, the catalytic activities were improved. The addition of MgO to Ni/SiO_2 showed remarkable inhibition effects on the catalytic activity, and increasing temperature to 350 °C or higher showed no promotion effects on the catalytic activity for se-Ni/Ca/Si catalyst. In comparison, SrO and BaO improved both the catalytic activity and CH_4 selectivity. Compared with Ni/Si catalyst, less metallic Ni species were presented on the SrO and BaO modified catalysts, which indicated that the SrO and BaO should be responsible for the superior catalytic performances of se-Ni/Sr/Si and se-Ni/Ba/Si catalysts. However, MgO addition demonstrated remarkable negative effects on the catalytic activity due to the very low reducibility of the metallic Ni species [19].

Table 3 Catalytic performance of alkaline-earth metal-modified Ni catalysts at different temperatures. Reaction conditions: GHSV = 15000 ml h^{-1} g^{-1}; H_2/CO_2 molar ratio = 4; P = 1 atm.

Samples	300 °C			350 °C			400 °C			450 °C		
	X_{CO_2}	S_{CH_4}	S_{CO}	X_{CO_2}	S_{CH_4}	S_{CO}	X_{CO_2}	S_{CH_4}	S_{CO}	X_{CO_2}	S_{CH_4}	S_{CO}
Ni/Si	27.0	94.5	5.5	64.7	97.5	2.5	73.2	98.7	1.3	70.8	95.5	4.5
se-Ni/Mg/Si	8.7	87.1	12.9	34.9	85.3	14.7	61.9	92.1	7.9	62.0	90.1	9.9
se-Ni/Ca/Si	37.2	97.2	2.8	64.9	98.6	1.4	73.3	98.9	1.1	70.6	95.4	4.6
se-Ni/Sr/Si	39.4	97.6	2.4	70.5	98.9	1.1	76.3	99.0	1.0	72.4	97.5	2.5
se-Ni/Ba/Si	38.3	97.4	2.6	67.6	98.5	1.5	74.9	98.9	1.1	72.2	97.3	2.7

3.6 Stability test

The research of catalyst stability tests had become an important issue in CO_2

methanation to realize its industrialized application. As for CO_2 methanation, its fatal drawback was that the catalysts were mainly subjected to the deactivation mechanisms caused by the sintering and/or oxidation of the metallic phase, which could lead to the decrease of the active metal sites on the catalyst surface and ultimately influence the catalyst stability. Therefore, the several catalyst performances at 50 h were monitored by means of CO_2 conversions of and CH_4 selectivities. The evaluation of the long-term catalyst stabilities was performed under specific reaction conditions: 350 ^oC, GHSV = 15000 ml h^{-1} g^{-1}, H_2/CO_2 molar ratio = 4 and P = 1 atm. The Ni/Si, se-Ni/Sr/Si and se-Ni/Ba/Si catalysts were selected as the typical catalysts. The results of catalyst stability and deactivation were shown in Fig. 6. As shown in Fig. 6, at the beginning, Ni/Si, se-Ni/Sr/Si and se-Ni/Ba/Si catalysts exhibited of 64.7, 70.5 and 67.6 % conversions to CO_2 and 97.5, 98.9 and 98.5 % selectivities to CH_4 at 0.5 h. In addition, compared to Ni/Si and se-Ni/Ba/Si catalysts, se-Ni/Sr/Si catalyst exhibited higher CO_2 conversions, higher CH_4 selectivities and more stable catalytic behavior in the whole 50 h time on stream [7,19]. At 50 h, CO_2 conversions of Ni/Si, se-Ni/Sr/Si and se-Ni/Ba/Si catalysts were 59.0, 65.5 and 59.7 % to and CH_4 selectivities of these catalysts were 95.4, 97.7 and 97.2 %, respectively. It indicated that se-Ni/Sr/Si catalyst might be better candidate as compared to Ni/Si and se-Ni/Ba/Si catalysts. Therefore, SrO addition was a more effective method to promote the catalytic performances.

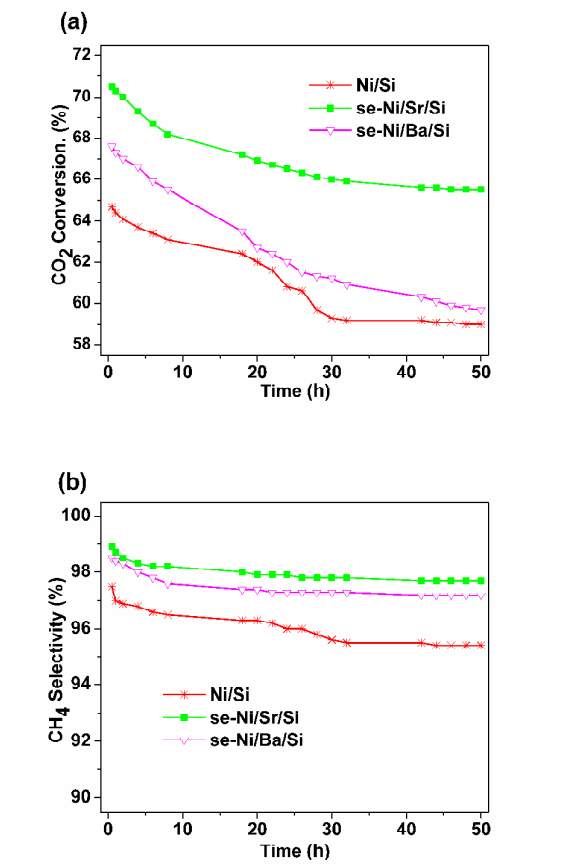

Fig. 6 Long-term stability tests at 350 °C. Reaction conditions: GHSV = 15000 ml h^{-1} g^{-1}; H_2/CO_2 molar ratio = 4; P = 1 atm.

The XRD patterns of the selected catalysts after 50 h reaction were comparatively plotted in Fig. 7. Compared to the reduced Ni/Si and se-Ni/Ba/Si catalysts, the average particle sizes of Ni phases in the used catalyst increased by about 10.7 and 8.1 nm, and the intensities of Ni and NiO phases decreased to 4.45 and 3.55, respectively. It indicated that not only the metallic Ni phase sintered, but the metallic Ni species on the catalyst surface could oxidize to NiO in the reaction process, which lower the catalytic stability. The metallic Ni particle size of the used se-Ni/Sr/Si catalyst estimated from XRD of the peaks at 2θ = 44.5° was 41.9 nm, and the intensities of Ni and NiO phases were 3.88. It demonstrated that in the reaction

process, modified SrO could inhibit the sintering of metallic Ni on the catalyst surface to some extent, which was in agreements with the results of stability test. Moreover, the diffraction peaks located at 2θ = 25.2, 36.3 and 50.0° (JCPDC Card No. 01-0556) indicated the existence of the characteristics of $SrCO_3$ phase, which might lead to the reduction of NiO species. Moreover, for CO_2 methanation, catalyst surface restructuring might be influenced by the feed gases [45], products [46,47], new species [48], and so on. In addition, the combination of metal cultures and particles on the Sr-based oxides were frequently reported [49-51]. With the help oxygen affinity, Ni atoms could react with substrate O atoms, resulting in reduction of high interfacial strain [52,53].

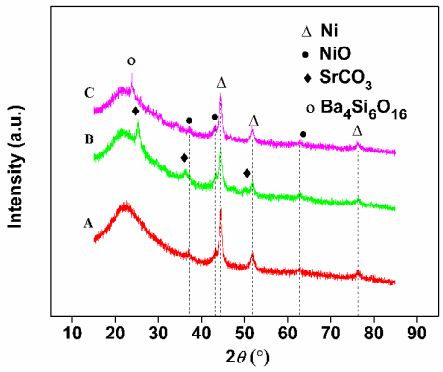

Fig. 7 XRD patterns of used Ni-based catalysts at 350 °C after 50 h: A, Ni/Si; B, se-Ni/Sr/Si; C, se-Ni/Ba/Si

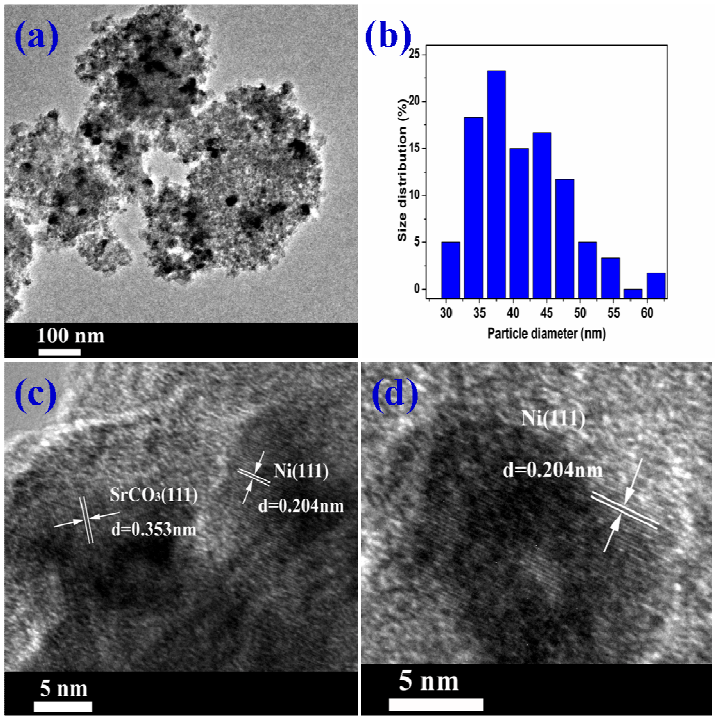

Fig. 8 (a) Low magnification, and (c, d) high magnification TEM images of the 50 h endurance-tested se-Ni/Sr/Si catalyst at 350 ^{o}C; (b) size distribution obtained from (a).

To understand further the roles of the SrO addition in the used se-Ni/Sr/Si catalyst, TEM analysis of the 50 h endurance-tested catalyst at 350 ^{o}C was carried out. As shown in Fig. 8a and b, the average size of Ni particles in the used se-Ni/Sr/Si catalyst was 37.5 nm based on 100 particles, which was very similar to the value estimated by XRD. These indicated further that the presence of SrO could inhibit the metallic Ni sintering. The *d*-spacings of Ni(111) and $SrCO_3$(111) were also given in Fig. 8c and d. These results might also demonstrate that the reason of the NiO species reduction in the reaction process was the formation of $SrCO_3$ phase.

4 Conclusion

Carbon dioxide methanation reaction had been studied over a series of Ni/SiO_2 catalysts modified with alkaline-earth metal oxides (MgO, CaO, SrO and BaO). MgO

addition inhibited the catalytic property of se-Ni/MgO/Si catalyst significantly due to the low reducibility of nickel species. The presence of CaO addition affected the reaction performance negligibly. However, SrO modification promoted the catalytic activity, and enhanced the catalyst stability because of the inhibition of the metallic Ni sintering. Moreover, BaO addition enhanced the catalytic activity, but se-Ni/Ba/Si catalyst deactivated dramatically because of the sintering of metallic Ni phase.

Acknowledgements

This work has been supported by the 973 Program and 863 Program of the Department of Sciences and Technology China (Grant Nos. 2013CB632404 and 2012AA051501); by the National Natural Science Foundation of China (21373245).

References

1 J. Gao, Y. Wang, Y. Ping, D. Hu, G. Xu, F. Gu and F. Su, *RSC Adv.*, 2012, **2**, 2358–2368.

2 B. Lu and K. Kawamoto, *RSC Adv.*, 2012, **2**, 6800–6805.

3 O. G. Griffiths, R. E. Owen, J. P. O'Byrne, D. Mattia, M. D. Jones and M. C. McManus, *RSC Adv.*, 2013, **3**, 12244–12254.

4 F. Ding, A. Zhang, M. Liu, X. Guo and C. Song, *RSC Adv.*, 2014, **4**, 8930–8938.

5 F. Wang, S. Zhang, C. Li, J. Liu, S. He, Y. Zhao, H. Yan, M. Wei, D. G. Evans and X. Duan, *RSC Adv.*, 2014, **4**, 10834–10840.

6 Z. Liu, Y. Wang, J. Li and R. Zhang, *RSC Adv.*, 2014, **4**, 13280–13292.

7 Z. Shen, M. Gu, M. Zhang, W. Sang, X. Zhou, Y. Zhang and F. Jin, *RSC Adv.*, 2014, **4**, 15256–15263.

8 W. Zhen, B. Li, G. Lu and J. Ma, *RSC Adv.*, 2014, **4**, 16472–16479.

9 Y. Li, G. Lu and J. Ma, *RSC Adv.*, 2014, **4**, 17420–17428.

10 W. Wang, S. Wang, X. Ma and J. Gong, *Chem. Soc. Rev.*, 2011, **40**, 3703–3727.

11 S. Sharma, Z. Hu, P. Zhang, E. W. McFarland and H. Metiu, *J. Catal.*, 2011, **278**, 297–309.

12 A. Karelovic and P. Ruiz, *J. Catal.*, 2013, **301**, 141–153.

13 D. J. Darensbourg, C. Ovalles and C. G. Bauch, *Rev. Inorg. Chem.*, 1985, **7**, 315–339.

14 J. L. Falconer and A. E. Zagli, *J. Catal.*, 1980, **62**, 280–285.

15 G. Du, S. Lim, Y. Yang, C. Wang, L. Pfefferle and G. L. Haller, *J. Catal.*, 2007, **249**, 370–379.

16 F. Ocampo, B. Louis, L. Kiwi-Minsker and A. C. Roger, *Appl. Catal. A: Gen.*, 2011, **392**, 36–44.

17 J. Liu, C. Li, F. Wang, S. He, H. Chen, Y. Zhao, M. Wei, D. G. Evans and X. Duan, *Catal. Sci. Technol.*, 2013, **3**, 2627–2633.

18. Q. Pan, J. Peng, S. Wang and S. Wang, *Catal. Sci. Technol.*, 2014, **4**, 502–509.

19 G. Meng and G. Lu, *Catal. Commun.*, 2014, **54**, 55–60.

20 G. D. Weatherbee and C. H. Bartholomew, *J. Catal.*, 1984, **87**, 352–362.

21 J. Lahtinen, T. Anraku and G. A. Somorjai, *Catal. Lett.*, 1994, **25**, 241–255.

22 S. Alayoglu, S. K. Beaumont, F. Zheng, V. V. Pushkarev, H. Zheng, V. Iablokov, Z. Liu, J. Guo, N. Kruse and G. A. Somorjai, *Top. Catal.*, 2011, **54**, 778–785.

23 G. Zhou, T. Wu, H. Xie and X. Zheng, *Int. J. Hydrogen Energy*, 2013, **38**, 10012–10018.

24 D. J. Dwyer and G. A. Somorjai, *J. Catal.*, 1978, **52**, 291–301.

25 A. E. Aksoylu, Z. Misirli and Z. I. Onsan, *Appl. Catal. A: Gen.*, 1998, **168**, 385–397.

26 J. Sehested, K. E. Larsen, A. L. Kustov, A. M. Frey, T. Johannessen, T. Bligaard, M. P. Andersson, J. K. Norskov and C. H. Christensen, *Top. Catal.*, 2007, **45**, 9–13.

27 A. C. Gluhoi, N. Bogdanchikova and B. E. Nieuwenhuys, *J. Catal.*, 2005, **232**, 96–101.

28 D. Yang, J. Li, M. Wen and C. Song, *Catal. Today*, 2008, **139**, 2–7.

29 L. Xu, H. Song and L. Chou, *ACS. Catal.*, 2012, **2**, 1331–1342.

30 J. Park and E. W. McFarland, *J. Catal.*, 2009, **266**, 92–97.

31 H. Y. Kim, H. M. Lee and J. Park, *J. Phys. Chem. C*, 2010, **114**, 7128–7131.

32 L. Xu, H. Song and L. Chou, *Int. J. Hydrogen Energy*, 2013, **38**, 7307–7325.

33 G. Larsen and G. L. Haller, *Catal. Lett.*, 1989, **3**, 103–110.

34 P. Panagiotopoulou and D. I. Kondarides, *Appl. Catal. B: Environ.*, 2011, **101**, 738–746.

35 F. Wang and G. Lu, *J. Phys. Chem. C*, 2009, **113**, 17070–17075.

36 K. Hadjiivanov, M. Mihaylov, D. Klissurski, P. Stefanov, N. Abadjieva, E. Vassileva and L. Mintchev, *J. Catal.*, 1999, **185**, 314–323.

37 S. Tomiyama, R. Takahashi, S. Sato, T. Sodsawa and S. Yoshida, *Appl. Catal. A: Gen.*, 2003, **241**, 349–361.

38 F. Pompeo, N. N. Nichio, M. G. Gonzalez and M. Montes, *Catal. Today*, 2005, **107**, 856–862.

39 Y. Pan, C. Liu and P. Shi, *J. Power Sources*, 2008, **176**, 46–53.

40 E. Lv, H. Zhang, Y. Yang and J. Ren, *J Mol Catal(China)*, 2012, **26**, 333–339.

41 S. Shi, Y. Wang, J. Ma, L. Zheng, R. Yao and L. Zhou, *J. Mol. Catal.(China)*, 2013, **27**, 539–547.

42 R. B. Shalvoy, P. J. Reucroft and B. H. Davis, *J. Catal.* 1979, **56**, 336–48.

43 F. Ocampo, B. Louis and A. C. Roger, *Appl. Catal. A: Gen.*, 2009, **369**, 90–96.

44 Z. Li, X. Hu, L. Zhang, S. Liu and G. Lu, *Appl. Catal. A: Gen.*, 2012, **417**, 281–289.

45 K. J. Williams, A. B. Boffa, J. Lahtinen, M. Salmeron, A. T. Bell and G. A. Somorjai, *Catal. Lett.*, 1990, **5**, 385–394.

46 M. P. Andersson, F. Abild-Pedersen, I. N. Remediakis, T. Bligaard, G. Jones, J. Engbæk, O. Lytken, S. Horch, J. H. Nielsen, J. Sehested, J. R. Rostrup-Nielsen, J.K. Norskov and I. Chorkendorff, *J. Catal.*, 2008, **255**, 6–19.

47 H. Olcay, Y. Xu and G. W. Huber, *Green Chem.*, 2014, **16**, 911–924.

48 M. Kilo, M. Hund, G. Sauer, A. Baiker and A. Wokaun, *J. Alloys Compd.*, 1996, **236**, 137–150.

49 Z. Zhang, J. Feng, Z. Wang, F. Yang, Q. Guo and J. Guo, *J. Chem. Phys.*, 2011, **236**, 144702.

50 A. Biswas, P. B. Rossen, C. Yang, W. Siemons, M. Jung, I. K. Yang, R. Ramesh and Y. H. Jeong, *Appl. Phys. Lett.*, 2011, **98**, 051904.

51 F. Sanchez, C. Ocal and J. Fontcuberta, *Chem. Soc. Rev.*, 2014, **43**, 2272–2285.

52 D. Vlachos, M. Kamaratos, S. D. Foulias, C. Argirusis and G. Borchardt, *Surf. Sci.*, 2004, **550**, 213–222.

53 M. Tanaka, *Appl. Surf. Sci.*, 2014, **98**, 324–329.